Directing crystallization outcomes of conformationally flexible molecules: polymorphs, solvates and desolvation pathways of fluconazole

*Maciej Nowak[1], Aleksandra J. Dyba[1], Jan Janczak[2], Alexander Morritt[3], László Fábián[3], Bożena Karolewicz[1], Yaroslav Z. Khimyak[3], Doris E. Braun[4], Karol P. Nartowski[1]**

1. Department of Drug Form Technology, Wroclaw Medical University, ul. Borowska 211, 50-556 Wroclaw, Poland

2. Institute of Low Temperature and Structure Research, Polish Academy of Sciences, P.O. Box 1410, Okólna 2 str., 50-950 Wroclaw, Poland

3. School of Pharmacy, University of East Anglia, Norwich Research Park, NR4 7TJ Norwich, UK

4. Institute of Pharmacy, University of Innsbruck, Innrain 52c, 6020 Innsbruck, Austria

KEYWORDS: fluconazole; polymorphism; solvates; desolvation; crystal structure

ABSTRACT

Control over polymorphism and solvatomorphism in API assisted by structural information, e.g. molecular conformation or associations via hydrogen bonds, is crucial for the industrial development

of new drugs, as the crystallization products differ in solubility, dissolution profile, compressibility or melting temperature. The stability of the final formulation and technological factors of the pharmaceutical powders further emphasize the importance of precise crystallization protocols. This is particularly important when working with highly flexible molecules with considerable conformational freedom and a large number of hydrogen bond donor or acceptors (*e.g.* fluconazole, FLU). Here, cooling and suspension crystallization were applied to access polymorphs and solvates of FLU, a widely used azole antifungal agent with high molecular flexibility and several reported polymorphs. Each of four polymorphic forms – FLU I, II, III, or IV – can be obtained from the same set of alcohols (MeOH, EtOH, isPrOH) and DMF *via* careful control of the crystallization conditions. For the first time two types of isostructural channel solvates of FLU were obtained (nine new structures). Type I solvates were prepared by cooling crystallization in Tol, ACN, DMSO, BuOH, and BuON. Type II solvates formed in DCM, ACN, nPrOH, and BuOH during suspension experiments. We propose desolvation pathways for both types of solvates based on the structural analysis of the newly obtained solvates and their desolvation products. Type I solvates desolvate to FLU form I by hydrogen bonded chains rearrangement. Type II solvates desolvation leads firstly to an isomorphic desolvate, followed by a phase transition to FLU form II through hydrogen bonded dimers rearrangement. Combining solvent mediated phase transformation with structural analysis and solid-state NMR supported by periodic electronic structure calculations allowed us to elucidate the interrelations and transformation pathways of FLU.

Introduction

Polymorphism and solvate formation of Active Pharmaceutical Ingredients (API) are important phenomena in drug development and formulation of new medicines. Polymorphs differ in physical properties, e.g. solubility, dissolution profile, compressibility, or manufacturability which can lead to radical changes in biopharmaceutical characteristics.[1] Considering the use of organic

solvents, a suitable drying procedure needs to be applied to avoid the presence of residual solvents in manufactured raw materials and final drug products in accordance with the ICH Q3C guideline.[2,3] Solvents used in purification protocols and the formulation process can also influence crystal structure of the final product. Moreover, the solvate desolvation process can provide access to novel polymorphic forms unreachable via other crystallization techniques such as melt crystallization or pressure induced phase transformation.[4]

Despite the substantial advancement of crystal structure prediction (CSP) and other computational methods, standard solvent mediated techniques are still extensively used in polymorph and solvate screening. Understanding the key interactions involved in nucleation and crystal growth is at the heart of crystal engineering. When crystallizing from a solvent many parameters influence the obtained polymorph, such as solution supersaturation, dynamics of temperature changes, or pressure. Formation of different polymorphs is also strongly related to solvent properties, e.g., the number of hydrogen bond donor and acceptor groups, hydrogen bond forming propensity, polarity, or viscosity. Mirmehrab *et al.*,[5] using ranitidine and stearic acid, revealed that formation of polymorphic forms can be correlated to partial charges and hydrogen bonding propensity of the solvent. She *et al.*[6] explored the connection between the occurrence of two polymorphic forms of undecylenic acid and the hydrogen bond donating ability of different solvents. Similar observations were made by Du *et al.*[7] and Zhang *et al*.[8] in studies on reactive crystallization of prasugrel and clopidogrel where the hydrogen bond donor propensity was identified as a crucial solvent property enabling access to different polymorphic outcomes. Results of our recent work[9] show that solution mediated phase transformation of acyclovir is favored in alcohols of high polarity and DMF. However, solvent properties are not always sufficient to explain crystallization outcomes. Mattei *et al*.[10] described the crystallization of two polymorphic forms of tolfenamic acid in ethanol, emphasizing the role of molecular conformation, as well as the influence of solute-solvent and solute-solute interactions on the nucleation of polymorphic forms. Distinct crystal structures of the well-known polymorph-rich

compound ROY (red-orange-yellow), a precursor to the antipsychotic drug olanzapine, were obtained from the same solvent.[11,12] Herein, the emphasis should be put on the simultaneous growth of two or more polymorphic forms (also in cocrystal systems[13]) or a mixture of polymorphs and solvates[14], referred to as concomitant crystallization. As this phenomenon remains poorly understood, it is crucial to follow strict crystallization procedures, especially for conformational polymorphs/solvates.[15]

Formerly solvates were mainly considered as by-products in the synthesis procedure and, due to safety and stability requirements, few API are marketed in solvated forms.[16] With an increasing interest in solvates as precursors for the synthesis of novel polymorphic forms, more effort is put into understanding the influence of API interactions with guest solvent molecules on the crystallization outcome, stability of multicomponent systems, and desolvation pathways. During desolvation either a phase transition with significant molecular rearrangement or formation of an isomorphic desolvate with only minor changes in the structure may occur. The tendency to solvate formation is explained primarily by two hypotheses. (i) Potential intermolecular interactions in the neat form e.g., hydrogen bonds, do not provide an optimal degree of lattice stability, hence solvents with hydrogen bond donor and/or acceptor capacity can be incorporated into the structure and create stronger interactions. (ii) Solvent inclusion decreases void space, which may lead to more efficient space filling.[17,18] Apart from intermolecular interactions the size and shape of solvent molecules were also identified as important factors in the mechanism of solvate formation. Braun *et al.* found that monosolvates and hemisolvates of dapsone are formed depending on the molecular volume of the solvent molecules - 83-146 $Å^3$ and 64-92 $Å^3$ respectively.[19] Yang *et al.* explained the formation of isostructural azoxystrobin solvates using solvents with molar volume between 56.1 and 88.5 cm^3/mol, however, larger molecules with linear shape (e.g., butyl acetate) can also be incorporated into the channel structure with a change in solvent stoichiometry.[20] Apart from the aforementioned aspects of solvate

formation, polymorphism in multicomponent systems should be considered, especially in relation to systems with maintained stoichiometry, so called true polymorphs.[21]

A recent study from Takieddin *et al.*[22] identified that the size and branching of the molecules as well as hydrogen bonding ability are the most important chemical properties that contribute to solvate formation of organic, nonionic, and nonpolymeric molecules. As structural complexity and median molecular mass of approved oral drugs has increased from *ca*. 305 Da for molecules registered before 1983 to nearly 430 Da for oral drugs discovered after 1990, solvate formation will continue to be a vital part of pharmaceutical drug discovery.[23]

In this work we evaluate directing crystallization outcomes of the solvate-forming and conformationally flexible API fluconazole (FLU) (2-(2,4-difluorophenyl)-1,3-bis(1,2,4-triazol-1-yl)propan-2-ol) which is one of the most widely used antifungal agents listed in WHO Model List of Essential Medicines.[24,25] FLU is classified among azole compounds - a prominent group of API widely used in the treatment of fungal infections. Their solubility, permeability, and activity are altered by the presence of various aryl halide and heterocyclic substituents.[26] Hence, understanding the key factors of crystallization and solvent mediated phase transformation of FLU and applying that knowledge to structurally related compounds may contribute to further development of anti-fungal agents, both in the pharmaceutical and agrochemical industry. FLU's six rotatable (Fig. 1) bonds make it a flexible molecule with significant conformational freedom, despite its small molecular size. Said flexibility, as well as one hydrogen bond donor and six hydrogen bond acceptor groups, establish FLU as a good model compound for examining the interplay between structural characteristics along with solvent properties in the light of polymorph and solvate formation. Since FLU was patented in 1983 by Richardson *et al.*[27], several studies concerning FLU polymorphism have been published, reporting up to nine polymorphic forms of FLU with five of them deposited in the Cambridge Structural Database (CSD ref. codes IVUQOF[28], IVUQOF01[29], IVUQOF02[29], IVUQOF03[29], and IVUQOF04[29]) (Table 1.). Extensive studies were also performed on the FLU monohydrate (CSD ref.

code IVUQIZ[28]). Recently the influence of crystal structure and molecular conformation on the FLU hydrate formation and desolvation was described in great detail.[30,31] Although a comprehensive overview of the reported polymorphs and preparation techniques was performed by Karanam *et al.*[29], some nuances related to the reported crystallization procedures may have caused literature discrepancies in the FLU polymorph nomenclature (ESI Table S1 presents numbering of FLU polymorphs as reported in available papers and supplemented by our findings). Such discrepancies are common in the evaluation of complex cases of pharmaceutical polymorphism and in case of FLU they could arise from concomitant crystallization of four FLU polymorphs from the same set of solvents, addressed in this work for the first time. After careful comparison of the published X-ray diffraction data and infrared spectra, along with reproduction of the experimental protocols reported to date[28,29,32–34], we could distinguish five crystalline forms of FLU and identify other reported polymorphs as mixtures of these polymorphs and the FLU hydrate. Numerous cocrystals[35–38] of FLU were also identified alongside three solvates (with ethyl acetate[28], benzene, and acetone[32]).

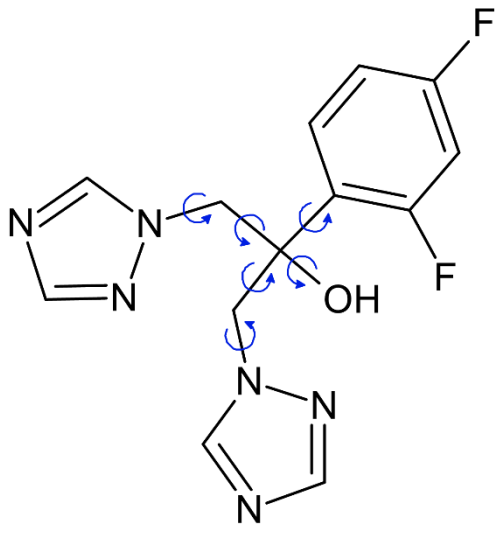

Figure 1. Molecular diagram of FLU, rotatable bonds marked with blue arrows.

Table 1. Structural data of FLU polymorphs and hydrate.

	Form I	Form II	Form III	Form IV	Form VI	Monohydrate
CSD code	IVUQOF02	IVUQOF04	IVUQOF	IVUQOF01	IVUQOF03	IVUQIZ
Space group	*Pbca*	*Pbca*	$P\bar{1}$	$P2_1/n$	$C2/c$	$P\bar{1}$
Unit cell parameters						
a/Å	12.9282(9)	10.9186(9)	7.4992(1)	6.6989(4)	27.4726(9)	5.6258(1)
b/Å	6.0241(5)	22.3367(18)	7.7869(1)	27.3867(19)	10.9196(4)	11.7373(2)
c/Å	34.834(3)	22.3619(17)	11.9817(2)	15.2901(11)	22.3424(12)	12.3063(3)
α/°	90	90	84.95(1)	90	90	71.24(1)
β/°	90	90	84.63(1)	90.319(3)	125.337(2)	79.87(1)
γ/°	90	90	75.89(1)	90	90	84.38(1)
Volume, Å^3	2712.9(4)	5453.74(8)	674.052(17)	2804.8(3)	5467.6(4)	756.63(3)
Z	8	16	2	8	16	2

With increasing structural complexity (and conformational flexibility) of newly synthesized drug candidates in pharmaceutical industry, directing the assembly of a desired solid form is a pressing research challenge. In this work we provide an example, how, by fine tuning of experimental conditions one can predictably and selectively yield four different polymorphs of FLU (form I, II, III, and IV) using a set of easily accessible alcohols (methanol, ethanol, and isopropanol) and *N,N*-dimethylformamide. Careful control of supersaturation (σ) and other crystallization conditions (eg. agitation, cooling rate and crystallization temperature) in 15 solvents selected based on their distinct properties[39] (ESI Table S2) enabled us to obtain new solvates and their polymorphs (type I and II solvates, nine new structures in total). The obtained phases were thoroughly characterized by thermal (DSC, TGA), spectroscopic (FTIR, solid-state NMR) and X-ray diffraction (both powder and single crystal) methods, corroborated with DFT calculations using CASTEP[40]. Through the analysis of molecular conformations, crystal packing, and hydrogen bonding motifs we were able to get an insight into structure-dependent stability and possible mechanisms of transitions between different forms of FLU. We propose desolvation pathways yielding selectively the FLU form I and FLU form II as desolvation products of type I and type II solvates, respectively. Furthermore, an isomorphous

desolvate was identified as the intermediate product on the desolvation path from type II solvates to FLU form II.

Materials and methods

Fluconazole (FLU) was a kind gift from Hasco Lek, Wroclaw, Poland. Due to the risk of hydration of the commercial sample (form I → monohydrate) if stored at ambient conditions, the material was dried in an oven at 130 °C for one hour before use. Solvents used in the study were of analytical grade and purchased from Sigma-Aldrich (acetone, 1-propanol, 2-propanol, 1-butanol, ethyl acetate, *N,N*-dimethylformamide, dimethyl sulfoxide, butanone) or J. T. Baker (acetonitrile, methanol, ethanol, dichloromethane, trichloromethane, toluene) and used directly.

Crystallization protocols (See Scheme 1 for the summary of the crystallization approaches used in this work):

Solubility measurements were carried out using high-performance liquid chromatography (HPLC, see section Solubility determination below and ESI Table S3) to determine FLU supersaturation in the used solvents. FLU:solvent ratios for the cooling and suspension crystallization experiments were based on the FLU solubility in each of the solvents.

Fluconazole form I (FLU I) is the commercially available form of FLU. It can be prepared via FLU hydrate desolvation (130°C, 1h in the oven) or via cooling crystallization (in ice bath) from FLU solutions in boiling isopropanol (isPrOH) at 50 mg/mL ($\sigma \approx 0.24$). Furthermore, FLU form I can also be obtained from methanol (MeOH), ethanol (EtOH), and *N,N*-dimethylformamide (DMF), although in these solvents concomitant crystallization with FLU form II may occur. Oven-dried commercial FLU was placed in 10 mL vials, followed by the addition of solvent (freshly opened) and the vials were tightly closed with caps. The suspension was heated above the boiling point of the solvent and

left to fully dissolve. The compositions of the starting mixtures were as follows (concentrations of FLU in crystallization solutions, as well as supersaturation, are provided in brackets with respect to solubility of form I at room temperature): 200 mg of FLU in 1 mL MeOH (200 mg/ml; $\sigma \approx -0.59$ at RT and $\sigma \approx 0.08$ at ice bath temperature), 200 mg of FLU in 1.5 mL EtOH (133 mg/ml; $\sigma \approx 0.29$), 100 mg of FLU in 2 mL of isPrOH (50 mg/ml; $\sigma \approx 0.24$) and 200 mg of FLU in 0.2 mL DMF (1000 mg/ml; $\sigma \approx 0.59$). Upon dissolution the samples were carefully removed from the heating plate, immediately placed in an ice bath (ice cubes with water) and left for crystallization (for 1 to 24 h). The obtained crystals were dried on a filter paper directly before the analysis.

Fluconazole form II (FLU II) was prepared by cooling crystallization from supersaturated (at room temperature, with respect to form I; for solubility data see ESI Table S3) FLU solutions. 500 mg of commercial FLU (form I) was dissolved in boiling solvents and resulted in supersaturated solutions: MeOH (500 mg/mL; $\sigma \approx 0.32$), EtOH (250 mg./mL; $\sigma \approx 0.91$), isPrOH (166 mg/mL; $\sigma \approx 1.44$), or DMF (1250 mg/mL; $\sigma \approx 0.81$) and left in closed vials for crystallization at room temperature. The obtained crystals were dried on a filter paper directly before the analysis.

Fluconazole form III (FLU III) was prepared by suspension crystallization at room temperature (RT, 22-24 °C) using commercial FLU form I. 200 mg of powdered and sieved (≤315 μm) FLU was used in crystallization studies. FLU was suspended in MeOH (0.3 mL), EtOH (0.3 mL), isPrOH (0.5 mL), and DMF (0.2 ml) at RT. The phase transition between FLU I and FLU III was observed in MeOH, EtOH, and DMF after 24-48 hours and in isPrOH after 96 hours. The obtained crystals were dried on filter paper directly before the analysis.

Fluconazole form IV (FLU IV) was prepared by suspension crystallization at RT using commercial FLU form I. 200 mg of powdered and sieved (≤315 μm) FLU was suspended in MeOH (0.3 mL), EtOH (0.3 mL), isPrOH (0.5 mL), or DMF (0.2 mL). Samples were stirred (300 rpm) at RT for 48 h (120 h for isPrOH). FLU form IV was also obtained using butanone (BuON) and dimethyl sulfoxide (DMSO). 500 mg and 1 g FLU were suspended in 5 mL of BuON and 1 mL of DMSO

respectively and stirred (300 rpm) for 14 days. Samples were analyzed after 7 and 14 days of solvent exposure. FLU crystals obtained in BuON were dried on filter paper before the analysis. After seven days in BuON the formation of FLU form III and after 14 days form IV was observed. DMSO samples were squeeze dried using a filter paper and subsequently dried in a desiccator for 48 hours before analysis. The formation of form IV in DMSO was observed after 14 days, without detectable formation of form III as an intermediate.

Type I fluconazole solvates: **acetonitrile solvate I (FLU ACN I), butanol solvate I (FLU BuOH I), toluene solvate (FLU TOL)**, **ethyl acetate solvate (FLU EtAc)**, and **butanone solvate (FLU BuON)** were prepared by dissolving commercial FLU in boiling solvents and then cooling the solutions. FLU (400 mg) was suspended in 5 mL of solvent (80 mg/mL, $\sigma \approx 0.25$-1.08 depends on FLU solubility in different solvents, see ESI Section S3) in a closed vial, heated to the boiling point of the solvent and stirred gently until dissolved. The obtained clear solution was cooled to RT and left for 1-2 hours to crystallize. The resulting crystals were dried on filter paper directly before the analysis. Due to the high solubility of FLU in DMSO, the **dimethyl sulfoxide solvate (FLU DMSO)** was prepared by dissolving 1 g of fluconazole in 700 µL of boiling DMSO (1420 mg/mL).

Type II fluconazole solvates: The **dichloromethane solvate (FLU DCM), n-propanol solvate (FLU PrOH)**, and **butanol solvate II (FLU BuOH)** were prepared by suspension crystallization for 1-2 weeks at RT using 500 mg of powdered fluconazole and 5 mL of solvent, except for FLU DCM solvate, where 3 mL of DCM were used. **Acetonitrile solvate II (FLU ACN II)** was prepared by suspension crystallization for 24 h using 500 mg of powdered fluconazole and 5 mL of ACN at 40-50 °C and additional stirring (300 rpm). The obtained materials were dried on filter paper directly prior to analysis.

Solubility determination[41]**:** Solubility of FLU form I was determined in all solvents (at 22-24 °C) apart from DCM, TCM, ACT and BuON due to an immediate start of phase transformation. As FLU

form I is not the thermodynamically favorable form in most used solvents, samples were collected after 10-60 minutes of vortexing and the FLU phase was identified by FTIR measurements to confirm the presence of FLU form I in the suspension. FLU solubility of polymorphs (I-IV) and both types of solvates at equilibrium was determined using HPLC (Agilent Infinity 1260, Agilent Technologies) (see ESI Table S3). The supersaturation (σ) was calculated using the following equation: $\sigma \approx \ln\left(\frac{C}{C^{sat}}\right)$, where C is the concentration and C^{sat} is the saturation concentration.[42] The solvent over an obtained form was collected, filtered using a 0.22 µm PTFE membrane filter and then diluted enabling HPLC determination of the FLU concentration. All measurements were performed on a Supelco Ascentis Express C18 column (10 cm x 4.6 cm) using a 10 µl sample injection volume. Both the samples and the column were kept at 30°C. A gradient HPLC method was used for the analysis with the UV-vis detector set for 255 nm wavelength. The mobile phase consisted of solvent A (water with a 0,1% addition of formic acid) and solvent B (acetonitrile) and the flow rate was 0.8 ml/min. The initial mobile phase composition was 90% A and 10% B, then changed to 2% A and 98 % B (7 minutes), held at that ratio for 2 minutes, then reversed back to 90% A and 10% B over the next 0.5 min and held for another 1.5 min for the chromatograph column equilibrium.

Powder X-ray diffraction: Powder X-ray diffraction patterns were acquired using a D2 PHASER Diffractometer (Bruker AXS, Karlsruhe, Germany) employing Cu Kα (1.5418 Å) radiation in the range of 2Θ between 5° to 36° and a low background holder. A step size of 0.02 ° and an irradiation time of 1.0 sec per step were used. The optics of the D2 PHASER diffractometer was a 2.5 ° Soller slit module system, a 0.2 mm divergence slit, a 1 mm air-scatter screen, and a Ni filter. The X-ray tube operated at 30 kV and 10 mA. Samples were carefully grinded using an agate mortar and a pestle. Due to the low stability of type I solvates, paraffin oil was used in the grinding process. Selected type II solvates and the isomorphous desolvates thereof were additionally analyzed using an X'Pert PRO diffractometer (PANalytical, Almelo, NL), equipped with a θ/θ coupled goniometer in transmission

geometry, programmable XYZ stage with well plate holder, Cu-K$\alpha_{1,2}$ radiation source and a solid state PIXcel detector. The patterns were recorded at a tube voltage of 40 kV and tube current of 40 mA, applying a step size of 2θ = 0.013° with 80 s (identification and time-resolved desolation) or 4000 s (structure solution) per step in the 2θ range between 2° and 40°/60°.

Structure solution from powder patterns:

The diffraction patterns of FLU DCM, FLU ACN II, and FLU nPrOH indexed to a tetragonal unit cell using the first twenty peaks with DICVOL04 and the space group was determined to be $P\bar{4}2_1c$ based on a statistical assessment of systematic absences,[43] as implemented in the DASH structure solution package.[44] Simulated annealing was used to optimize the three solvate models against the diffraction data set in direct space. The internal coordinate (Z-matrix) descriptions were derived from the PBE0/6-31G(d,p) gas phase global conformational minima with O–H distances normalized to 0.9 Å and C–H distances to 0.95 Å. Each of the structures was solved using 200 simulated annealing runs of 5 x 10^7 moves per run in DASH. Each FLU molecule was allowed 6 external and 5 internal degrees of freedom and nPrOH 6 external and 1 internal degree of freedom. The best solutions were subjected to CASTEP[40] optimizations and the resulting PBE-TS structures, with O–H distances normalized to 0.9 Å and C–H distances to 0.95 Å, were then used as the starting point for rigid body Rietveld refinements[45] in TOPAS V7.12.[46] The final refinements included a total of 41 (FLU DCM and FLU ACN II) and 48 parameters (FLU nPrOH). For more details, see section S8 of the Supporting Information.

Single crystal X-ray diffraction: X-ray intensity data for the crystals **FLU Tol**, **FLU ACN I**, and **FLU DMSO** were collected using graphite monochromatised MoKα radiation on a four-circle κ geometry KUMA KM-4 diffractometer with a two-dimensional CCD detector. The ω-scan technique with Δω = 1.0 ° for each image was used for data collection. One image was used as a standard after

every 40 images for monitoring of the crystal stability and data collection, and no correction on the relative intensity variations was necessary. Data collections were made at RT using the CrysAlis CCD program.[47] Integration, scaling of the reflections, correction for Lorenz, and polarization effects and absorption corrections were performed using the CrysAlis Red program.[47] The structure was solved by direct methods using SHELXT[48] and refined using the SHELXL-2018 program.[49] The hydrogen atoms were introduced in their geometrical positions and treated as rigid. The final difference Fourier maps showed no peaks of chemical significance.

Fourier transform infrared spectroscopy: FT-IR spectra were obtained with a Nicolet iS50 spectrometer (Thermo Scientific, USA) using the attenuated total reflectance (ATR) method. The spectra were recorded over a wavelength of 400 cm^{-1} to 4000 cm^{-1} at 32 scans per sample and a resolution of 4 cm^{-1}.

Solid-state NMR: All solid-state NMR spectra were acquired using a Bruker 400 MHz Avance III solid-state NMR spectrometer equipped with a triple resonance probe at frequencies 400.23 MHz (^{1}H), 376.57 MHz (^{19}F) and 100.64 MHz (^{13}C). FLU polymorphs and solvates were packed in the 4 mm zirconia rotors and rotated at a MAS rate of 10 kHz. All materials were characterized using ^{1}H–^{13}C cross-polarization magic angle spinning (CP/MAS) technique (^{1}H $\pi/2$ pulse length 3.5 μs, ^{13}C $\pi/2$ pulse length 3.5 μs, ^{1}H–^{13}C CP contact time 2 ms, SPINAL64 decoupling was used during signal acquisition). Optimized recycle delay was 120 s. The Hartmann–Hahn conditions for ^{1}H–^{13}C CP/MAS NMR experiment were set with hexamethylbenzene (HMB). Typically, 128 and 256 scans were acquired for Z' = 1 for Z' = 2 structures, respectively. The ^{13}C chemical shifts were recorded with respect to TMS. The assignment of the ^{13}C peaks was performed based on ^{1}H-^{13}C HSQC spectra in D_2O, ^{1}H-^{19}F CP/MAS, ^{1}H-^{13}C NQS spectra and CASTEP prediction of chemical shifts

Differential scanning calorimetry. DSC thermograms were recorded using the DSC 214 Polyma (Netzsch). Samples (4-5 mg) were weighed in sealed aluminum pans (25 μL) with pierced cover.

Measurements were carried out at a heating rate of 5 °C min^{-1} in the temperature range between 0 °C and 150°C in nitrogen atmosphere (25 mL min^{-1} flow rate). The onset temperatures of the melting and desolvation processes were determined using the Netzsch Proteus Analysis software.

Thermogravimetric analysis. The stoichiometric ratios of the solvates were determined using a Thermo-Microbalance TG 209 F1 Libra (Netzsch, Germany). Approximately 9-10 mg of the samples were placed in 150 μL Al_2O_3 crucibles and heated at a heating rate of 5 °C min^{-1} in the temperature range of 30-150 °C in nitrogen atmosphere (25 mL min^{-1}). The measurements were performed immediately after harvesting the crystals from the solutions. The obtained thermograms were analyzed using the Netzsch Proteus Analysis software.

Computational details. All computations were performed using CASTEP.[40] The cell files were generated using the CIF2cell tool based on the structures available in the CSD (ref. codes IVUQOF[28], IVUQOF01[29], IVUQOF02[29], IVUQOF03[29], and IVUQOF04[29]) and representative structures of both types of solvates (DMSO for type I and DCM for type II).[50] The geometry optimisation was performed with the Perdew– Burke–Ernzerhof (PBE) generalized gradient approximation (GGA) exchange correlation density functional[51] and ultrasoft pseudopotentials[52] with the addition of the Tkatchenko and Scheffler (TS) model[53]. The Monkhorst–Pack grid was sampled with 0.05 $Å^{-1}$ separation of k-points and cut-off energy of 800 eV, both optimised for convergence. Geometry optimization was performed with cell dimensions constrained. Chemical shifts were calculated using the gauge including projector augmented wave approach (GIPAW)[54,55] as implemented in the CASTEP code. The generated isotropic shielding constants (σ_{calc}) were converted to chemical shifts (δ_{calc}) according to the following equation: $\delta_{calc} = \sigma_{ref} - \sigma_{calc}$. The reference shielding constant value (σ_{ref}) was taken from the zero intercept of the fit of calculated shielding vs. experimental chemical shift plot $\sigma_{calc} = -x \cdot \delta_{exp} + \sigma_{ref}$.

Results and discussion

Selective crystallization of FLU polymorphs in alcohols.

In this study we were able to obtain four polymorphic forms of FLU (form I, II, III, IV) using cooling and suspension crystallization from methanol, ethanol, isopropanol, and *N,N*-dimethylformamide with careful manipulation of the experimental conditions and supersaturation levels. The differences in solubility of FLU forms (I-IV) in different solvents enabled us to better understand the effect of crystallization conditions on the resulting solid form of FLU (Fig. 2). Previously reported protocols[28,29,32,34,56] for the preparation of FLU polymorphs employed cocrystallization experiments or solution crystallization methods. However, the results of similar experiments performed by different groups showed inconsistencies.

FLU form I was first described by Gu *et al.*[57] (polymorph I) and Dash and Elmquist[58] (their polymorph II). Alkhamis *et al.*[32] prepared form I via crystallization from isPrOH, while Kreidl *et al.*[34,56] obtained form I using either cooling crystallization (from isPrOH or EtOH) or by temperature-induced desolvation of FLU monohydrate. This form was also found to be the most soluble in alcohols and DMF amongst all FLU polymorphs (Fig. 2). Careful comparison of experimental data of form I acquired in our work and the results published by others[32,34,56–58] indicates that the PXRD pattern of polymorph 5 reported by Karanam *et al.*[29] (ref. code IVUQOF2) corresponds to form I. Polymorph 5 was obtained in a failed cocrystallization experiment with glycolic acid in an ACN solution.[29] This polymorph was found to crystallize in the centrosymmetric orthorhombic *Pbca* space group with one molecule in the asymmetric unit (Z'=1). The conformation of FLU form I is stabilized by infinite hydrogen-bonded $C_1^1(7)$ chains along the *b* axis via O−H···N hydrogen bonds and π-stacking of triazole rings. Form I melts at 140.5-141.1 °C with a heat of fusion 34.5 ± 0.9 kJ/mol (ESI Fig. S6).

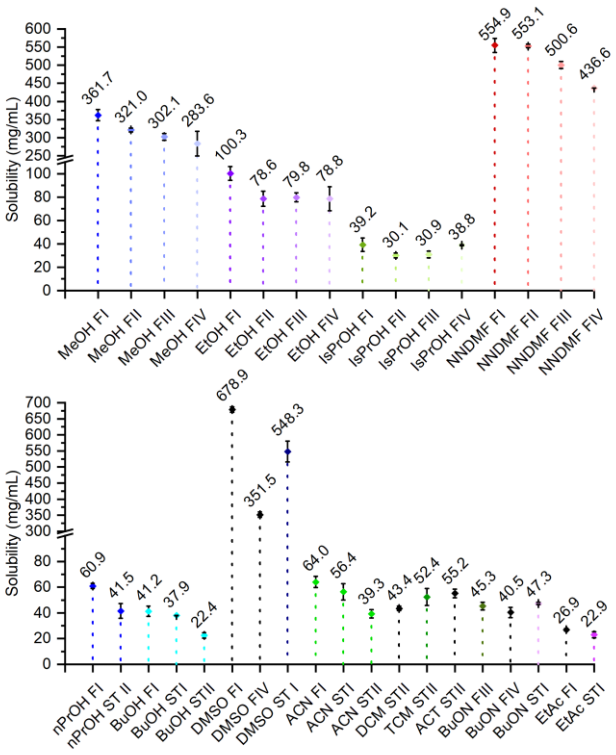

Figure 2. Solubility of fluconazole polymorphs and solvates in investigated solvents.

The second form, referred here to as FLU form II, was first obtained by Desai *et al.*[33] by recrystallisation from molten fluconazole. The low resolution PXRD patterns of the obtained crystals matched our PXRD pattern of FLU form II and the simulated pattern of polymorph 7 (ref. code IVUQOF04) obtained by Karanam *et al.*[29] in cocrystallization experiments (ESI Fig. S2). We monitored the crystallization of FLU from the melt *in situ* using variable temperature ^{1}H-^{13}C CP MAS solid-state NMR spectroscopy (ESI Fig. S3) and the spectrum at 90 °C, *i.e.* after cold crystallization of amorphous FLU at 77-80 °C (ESI Fig. S4) was in agreement with the solid-state NMR spectrum of form II obtained using solvent crystallization. FLU form II obtained from the melt displayed much lower crystallinity as compared to form II obtained from solvent as indicated via broadening of PXRD peaks (ESI Fig. S2). Furthermore, Karanam *et al.* obtained polymorph 7 (*i.e.*, the already described form II) from an isopropanol solution. This is in agreement with FLU crystallization experiments from isPrOH at $\sigma \approx 1.44$ performed in this work (ESI Fig. S7). This polymorph crystallizes in the centrosymmetric orthorhombic *Pbca* space group with two molecules in the asymmetric unit (Z'=2).

The molecules in the structure create hydrogen-bonded dimers $R_2^2(14)$ *via* O−H···N hydrogen bonds. Form II melts at 136.8-139.1 °C with heat of fusion 35.2 ± 1.0 kJ/mol (ESI Fig. S8).

PXRD diffractograms of the collected powders matched the diffractograms calculated for structures deposited in the CSD and were further supported by FTIR, ^{1}H-^{13}C CP-MAS NMR, thermal analysis and DFT calculated ^{13}C chemical shifts using CASTEP (Fig. 3). The simulated PXRD patterns of the obtained FLU form I (IVUQOF02) and FLU form II (IVUQOF04) were in agreement with the experimental PXRD traces (Fig. 3D, ESI Fig. S5;S7). FLU polymorphs show characteristic FT-IR spectra (Fig. 3E) for each form, especially in the 3200-2900 cm^{-1} region with peaks assigned to triazole C-H stretching, difluorophenyl C-H stretching and methylene C-H asymmetric stretching (for full peak assignment based on the work of Chandrasekaran *et al.*[59] see ESI Table S5). Conformational similarity of FLU molecules in these forms might account for the fact that polymorphs with notably distinct crystal packing can be obtained concomitantly from the same crystallization experiment. Overlapping of FLU conformers from the respective forms (Fig. 3B, Table 2) shows that only minor changes in torsion angles can be found amidst FLU form I, II, and III, as well as the hydrate. Only the triazole ring in FLU form IV adopts an explicitly different position. Furthermore, FLU forms I and II (as well as form III) are energetically close to each other as indicated by similar melting points (from 136.8 to 141.1 °C), heats of fusion (*ca.* 34.9 ± 0.7 kJ/mol) and solubilities. Therefore, it is not surprising that these forms can be obtained concomitantly. Solvent properties and intermolecular forces between the solute and the solvent affect the crystallization outcome, however, a particular emphasis on other crystallization conditions e.g., saturation, agitation, or temperature is essential in directing crystallization.[60]

The cooling crystallization of FLU from isPrOH at $\sigma \approx 0.24$ led to preferential formation of FLU form I. At a higher supersaturation of FLU ($\sigma \approx 1.44$) in isPrOH form II crystalizes selectively. In MeOH, EtOH, and DMF both forms, I and II, can be obtained concomitantly from MeOH ($\sigma \approx -0.59$), EtOH ($\sigma \approx 0.28$) and from DMF ($\sigma \approx 0.59$), while selective crystallization of form II is observed at

$\sigma \approx 0.32$ from MeOH; $\sigma \approx 0.91$ from EtOH, and $\sigma \approx 0.81$ from DMF. The presence of water also affects FLU crystallization due to both water activity as well as its effect on the supersaturation with respect to the FLU hydrate and anhydrous forms (see ESI Table S4 for solubility measurements and a_w values). For example, Basford *et al.*[30] found that FLU hydrate is formed in isopropanol at water activity (a_w) ranging from 0.2 to 0.3 depending on the starting form and the presence of FLU hydrate seeds. In our study we performed crystallization in isPrOH, EtOH, MeOH and DMF with addition of water (50-200 μL of water per 1 mL of a solvent) to investigate how the presence of water affects the crystallization outcome. In comparison to samples prepared using dry solvents, the addition of water significantly slowed the crystallization process from a few hours to even a few days as a consequence of increased FLU solubility in water mixtures with alcohols. The formation of the FLU hydrate was also observed in crystallization experiments from MeOH ($a_w = 0.37$), EtOH ($a_w = 0.70$), isPrOH ($a_w = 0.46$) and DMF ($a_w = 0.56$). This indicates that careful control over the RH conditions was essential for the selective crystallization of either form I or form II of fluconazole, especially for solvents with high tendency to sorb water from the environment.

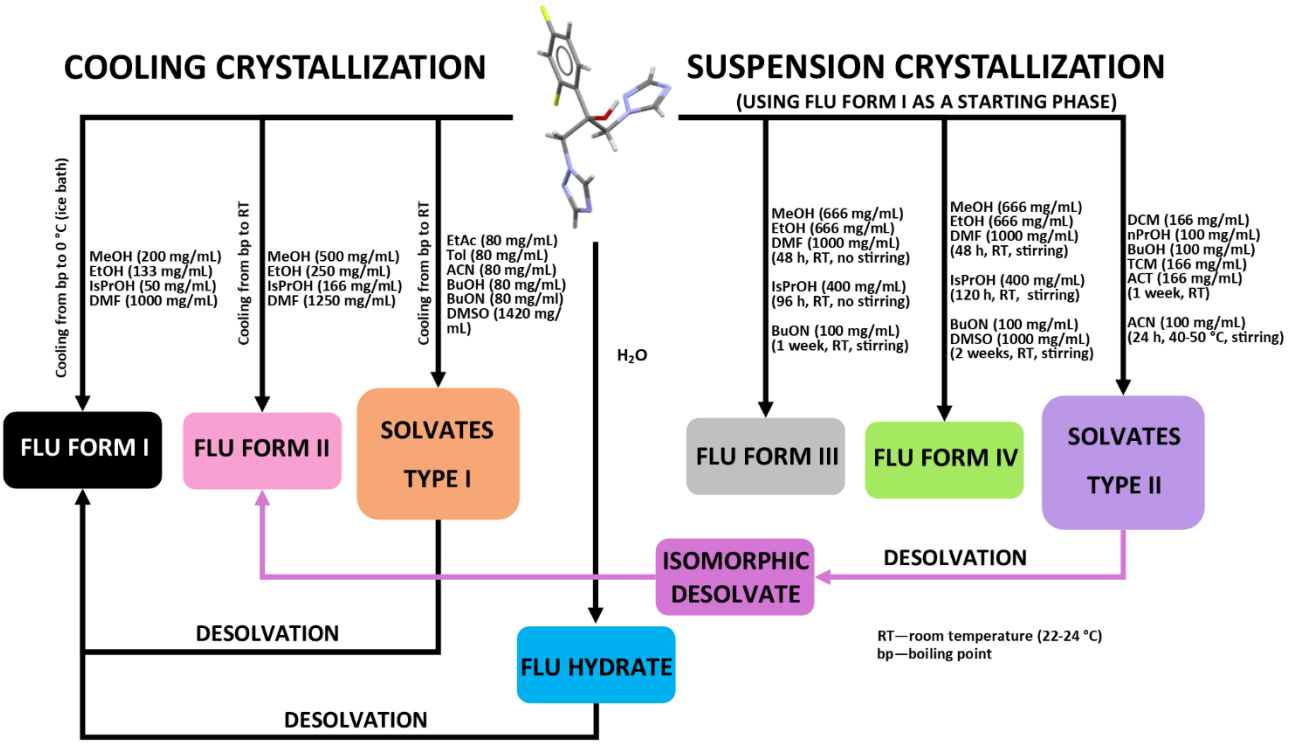

Scheme 1. Crystallization conditions and solvent mediated phase transitions of FLU.

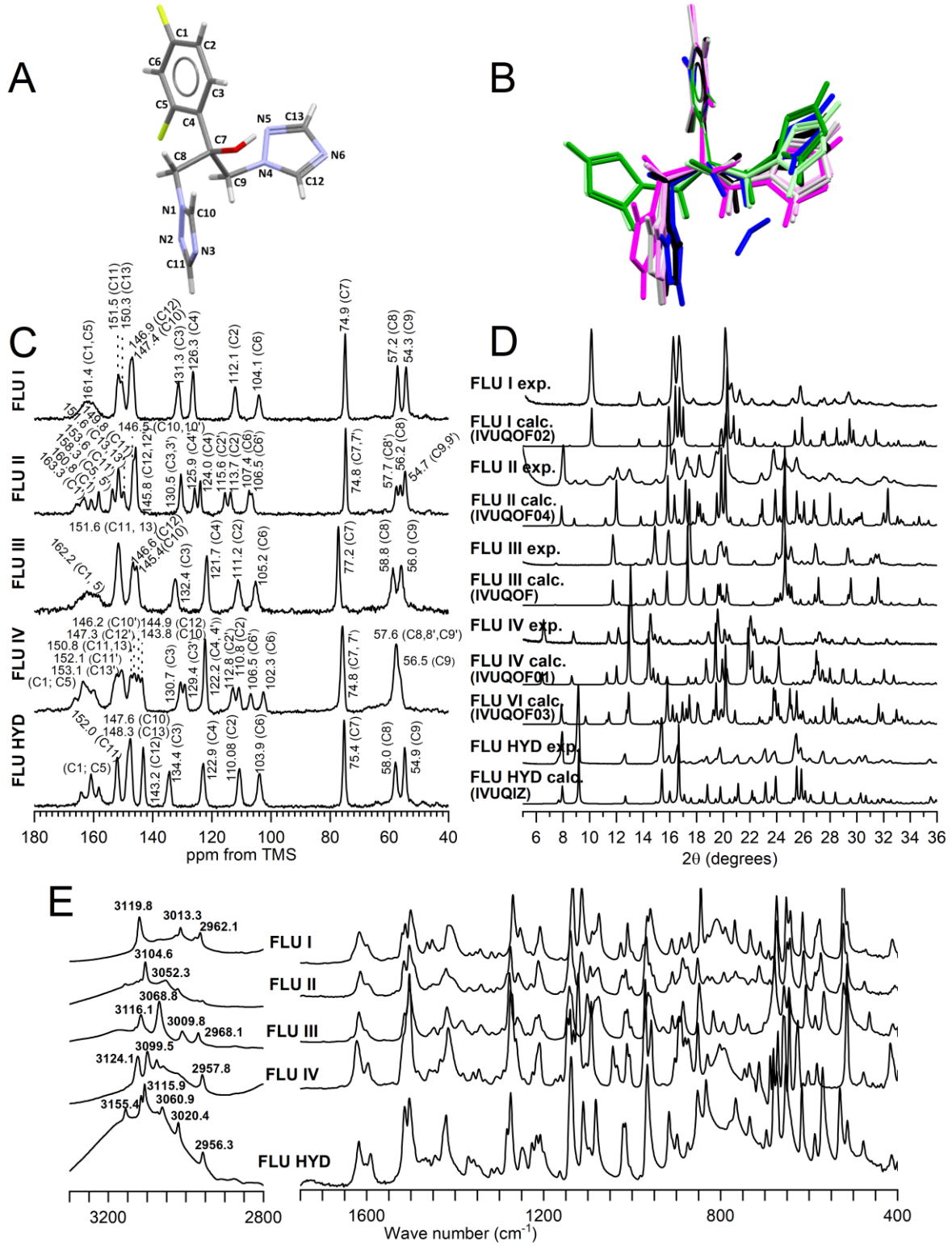

Figure 3. Structure of fluconazole with carbon and nitrogen atom labeling. B. Overlap of fluconazole conformations in polymorphs and the hydrate: FLU I – black, FLU II – pink and magenta, FLU III – gray, FLU IV – green and light green, the FLU hydrate – blue. C. ^{1}H-^{13}C CP/MAS NMR spectra of

fluconazole polymorphs and the hydrate. D. Experimental and calculated PXRD patterns of FLU I, FLU II, FLU III, FLU IV, FLU VI, and the FLU hydrate. E. FT-IR spectra of FLU polymorphs I, II, III, IV, and hydrate.

Table 2. List of selected torsion angles in fluconazole molecules present in forms I-IV and the hydrate.

	Form I	Form II	Form II'	Form III	Form IV	Form IV'	Hydrate
C3-C4-C7-O	-3.69°	-8.48°	5.01°	-8.1°	14.42°	14.57°	8.91°
C4-C7-C8-N1	-174.81°	-178.59°	-167.21°	165.95°	-64.53°	-65.38°	179.82°
C4-C7-C9-N4	68.27°	64.8°	69.16°	52.09°	55.6°	65.13°	52.9°
C7-C8-N1-N2	-89.65°	-90.58°	-86.91°	-101.23°	76.91°	79.26°	-101.14°
C7-C9-N4-N5	-73.1°	-84.14°	-79.78°	-99.67°	-83.96°	-91.82°	-102.07°
C7-C8-N1-C10	90.05°	88.67°	95.8°	71.92°	-102.31°	-101.85°	80.79°
C7-C9-N4-C12	103.27°	95.88°	97.05°	79.29°	92.7°	89.18°	73.09°

Using suspension crystallization of FLU from MeOH, EtOH, isPrOH and DMF we were able to obtain FLU form III. This form was first reported by Lo *et al.*[61] (their anhydrous form) in 1994. Nearly a decade later Caira *et al.*[28] obtained FLU form III by dissolving FLU in isPrOH at 40 °C followed by cooling of the obtained solution toRT, providing single crystal XRD, DSC and FT-IR data. A similar cooling crystallization method was used earlier by Kreidl *et al.*[34,56] where FLU form III (their Crystal Modification II) was obtained using isPrOH, EtOH, and 2-butanol. However, the procedures proposed by Caira *et al.* and Kreidl *et al.* always result in the formation of FLU form I or FLU form II in our experiments. FLU form III was found to crystallize in the centrosymmetric triclinic space group $P\bar{1}$ with Z'=1. Similarly to FLU form II, the molecules create hydrogen-bonded dimers $R_2^2(14)$ via O−H···N hydrogen bonding. Gathered experimental and simulated PXRD patterns (IVUQOF) are presented in the ESI (Fig S9). FLU form III melts at 138.4-140.9 °C with a heat of fusion 35.1 ± 0.3 kJ/mol (ESI Fig. S10).

FLU form IV was first obtained by Karanam *et al.*[29] as a byproduct in a cocrystallization experiment. Afterwards, a new solution-mediated crystallization protocol of FLU form IV was described by Basford *et al.*[30] They obtained FLU form IV by agitating a saturated butanone solution of 1:1 mixture of FLU form III (their AH-A form) and the monohydrate for seven days. In our study FLU IV was obtained in MeOH, EtOH, isPrOH, DMF, BuON, and DMSO using form I as a starting material in suspension crystallization with agitation in less than 4 days (MeOH, EtOH, isPrOH, DMF) or 14 days in DMSO. In the suspension experiments using BuON, with FLU form I as a starting material, formation of FLU form III was first observed after one week while an additional week of suspending resulted in the formation of FLU form IV. Both forms III and IV of FLU have very similar solubility in investigated solvents with form IV being the least soluble form in MeOH, EtOH, DMF and BuON (Fig. 2, ESI Table S3).

FLU form IV was found to crystallize in the centrosymmetric monoclinic $P2_1/n$ space group with Z'=2. Molecular conformation of FLU form IV, similarly to FLU form I, is stabilized by infinite O−H···N hydrogen-bonded chains $C_2^2(14)$ along the *a* axis. Collected PXRD patterns are corresponding to the calculated PXRD data (ESI Fig S11). FLU form IV melts at 137.4-139.9 °C with heat of fusion 38.9 ± 0.4 kJ/mol (ESI Fig. S12).

Solid-state NMR analysis of FLU polymorphs. The assignment of the ^{1}H-^{13}C CP/MAS solid-state spectra was based on NQS and ^{19}F-^{13}C CP/MAS as well as CASTEP calculated isotropic chemical shifts (ESI Table S6) for FLU forms I, II, III, IV, and the FLU hydrate. As FLU forms I, III, and the hydrate have one FLU molecule in the asymmetric unit and FLU forms II and IV have two FLU molecules in the asymmetric unit, 13 and 26 peaks were expected in the solid-state NMR spectra, respectively. Albeit, the very similar local environment of triazole ring carbons resulted in overlapping of ^{13}C peaks in the 155 to 140 ppm spectral region. We were unable to assign the aromatic carbons C1 and C5 due to peaks broadening, hence carbons C1 and C5 were omitted in the RMSD calculations. The experimental and calculated (CASTEP) ^{13}C NMR peaks positions were in

agreement as demonstrated by low RMSD values for the FLU polymorphs (below 2 ppm) and for the FLU hydrate (RMSD = 3.09 ppm). For detailed solid-state NMR analysis see ESI Section S6.

Fluconazole type I solvates

To date three FLU solvates: acetone[32], benzene[32], and ethyl acetate[28] have been reported and only for the latter the crystal structure was fully solved. Through the application of the cooling or suspension crystallization method, we obtained nine new solvates of FLU and based on their crystal structure similarity we divided them into two groups: type I and type II solvates (Scheme 1). From cooling crystallization experiments a set of type I solvates: FLU Tol, FLU ACN I, FLU DMSO, FLU BuOH I, and FLU BuON was obtained. It is important that strict time regimen and careful sample preparation are followed during the synthesis in order to obtain phase pure materials. This is because: i) FLU ACN I and FLU BuOH I solvates are not thermodynamically stable in a solution and they can transform into the second type of solvate within a couple of minutes, ii) during grinding for PXRD analysis type I solvates easily desolvate, leading to form I. Similar to the neat polymorphic forms, the relative humidity should be controlled and fresh or dried solvents should be used to avoid hydrate formation.

X-ray and crystal structure analysis. Type I FLU solvates were analyzed using PXRD (Fig. 4A). The crystal structures for three of the type I solvates (FLU Tol, ACN I and DMSO) were solved by SCXRD and the crystallographic data are summarized in Table 3. Comparison of the PXRD patterns of the new solvates and the known FLU EtAc solvate (IVUQEV) indicate that they are isomorphous and only minor differences between structures can be identified. Experimental PXRD patterns of type I solvates agree with the calculated PXRD patterns of the solvates FLU ACN I, FLU DMSO, and FLU Tol. FLU Tol crystalizes in *Iba*2, while FLU ACN I and FLU DMSO form *Pbcn* space group, with one FLU molecule in asymmetric unit (Z'=1). The FLU EtAc solvate reported by Caira *et al.*[28] has two FLU molecules in the asymmetric unit, which does not agree with ^{1}H-^{13}C CP/MAS solid-state NMR data as for this phase one peak per each carbon atom was observed (Figure 4B). This may

be related to temperature effects as NMR spectra were recorded at 20 °C while FLU EtAc crystal structure was solved at -80 °C. Crystal packing similarity calculation (Mercury CSD 2021.1.0) for solvates of type I shows that FLU EtAc, FLU ACN I, and FLU DMSO have 15 out of 15 FLU molecules in common which indicates that they form the same crystal structure with $RMSD_{15}$ in the range of 0.111-0.227 Å. For FLU Tol solvate 12 out of 15 molecules were found in common with the other type I solvates, the $RMSD_{15}$ range is 0.107-0.145 Å. Investigation of missed matches shows that a 2D packing motif is present with different symmetries relating the common slabs to each other in the two structures.

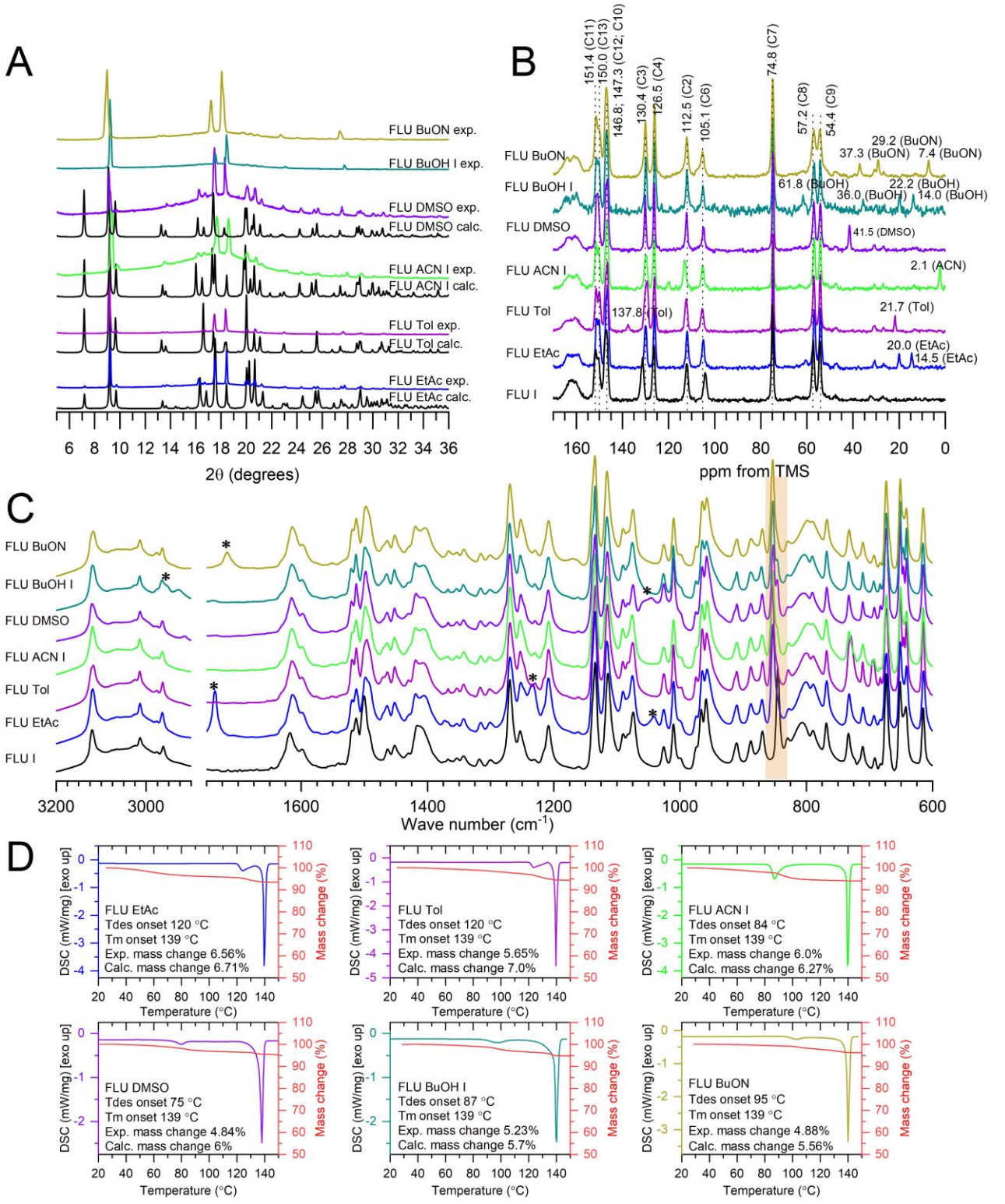

Figure 4. A. Experimental and calculated PXRD patterns of type I FLU solvates. B. ^{1}H-^{13}C CP/MAS NMR spectra of type I FLU solvates. C. FTIR spectra of type I FLU solvates with peaks assigned to the solvents marked with stars. D. DSC and TGA thermograms of type I FLU solvates.

Table 3. Structural data of FLU type I solvates.

	FLU EtAc[28]	FLU Tol	FLU ACN I	FLU DMSO
Empirical formula	$C_{13}H_{12}F_2N_6O \cdot 0.25(C_4H_8O_2)$	$C_{13}H_{12}F_2N_6O$	$C_{13}H_{12}F_2N_6O \cdot ½(CH_3C{\equiv}N)$	$C_{13}H_{12}F_2N_6O$
CSD ref. code or deposition CCDC No.	IVUQEV	CCDC 2111083	CCDC 2111082	CCDC 21110824
Space group	*P*21/*c*	*Iba*2	*Pbcn*	*Pbcn*
a/Å	6.0484	38.778(2)	38.462(2)	38.884(9)
b/Å	38.5004	13.0015(9)	13.0004(8)	13.0158(4)
c/Å	12.9698	6.1413(4)	6.1930(5)	6.1206(2)
α/°	90	90	90	90
β/°	90.22	90	90	90
γ/°	90	90	90	90
V, Å3	3020.1	3096.3(3)	3096.6(4)	3097.7(7)
Z	8	8	8	8

Similarly to FLU EtAc, the investigated solvates create channel structures where FLU molecules form a hydrogen bonded network of host molecules (Fig. 5A). Among the obtained solvates we were able to identify the position of disordered ACN molecules only with an occupancy of 0.25 in the structure, while the other solvents displayed increased mobility within the channels resulting in diffuse scattering in single crystal X-ray analysis. This likely results from the lack of hydrogen bonding between FLU and solvent molecules. Hence, after taking the crystals from the mother crystallization solution to air the solvent leaves the crystal. The molecular conformation of FLU in the type I solvates is stabilized by infinite hydrogen-bonded O−H···N C(7) chains and π-stacking of triazole rings (Fig. 5B). A very similar chain arrangement can be found in FLU form I. There are also

only minimal differences in torsion angles between FLU molecules in polymorph I and the solvate structures (Fig. 5C). These findings may rationalize the formation of FLU form I as the desolvation product of type I solvates since this transformation requires only a “simple” chain rearrangement (Fig. 5C-E)[62].

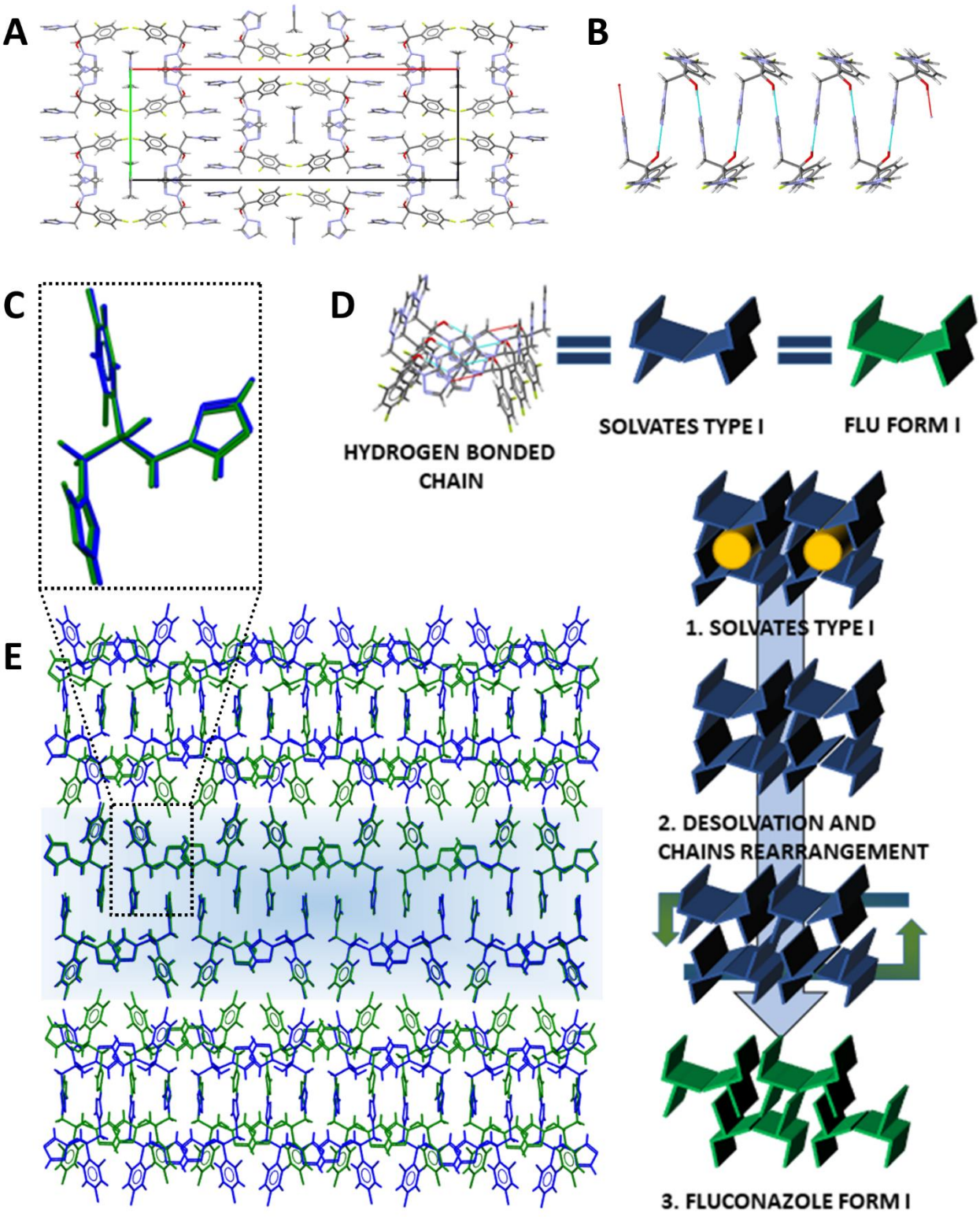

Figure 5. A. Packing of type I FLU solvates (as represented by FLU ACN I). B. Hydrogen bonded chain in type I solvates. C. Overlay of FLU conformations in form I (blue) and type I solvates (green). D. Proposed schematic representation of the rearrangement of chains during desolvation of FLU type

I solvates. E. Overlay of crystal packing of FLU form I (green) and FLU type I solvates (blue). The arrows indicate a possible rearrangement of FLU molecules during desolvation.

FTIR and solid-state NMR analysis. All analyzed FTIR spectra of type I solvates display similar peak positions and intensities resulting from the isostructurality of the examined materials (Fig. 4C, full peak assignment in ESI Table S5). The spectra of type I solvates are also similar to the spectrum of FLU form I. This can be explained both by the similar conformation of FLU molecules and by the common hydrogen bonding chains stabilizing the structures. The differences between the spectra of FLU form I and type I solvates are slight broadening of the peaks in the solvate spectra and one characteristic peak shifting between 855 and 840 cm^{-1} (assigned to the difluorophenyl ring C-H out-of-plane bending). We could also identify several peaks distinctive for solvent molecules (ESI Table S5). The ^{1}H-^{13}C solid-state NMR spectra of FLU type I solvates display very similar peak positions due to isostructurality of the obtained materials. The experimental and calculated chemical shifts for FLU DMSO solvate agreed with a RMSD value equal to 1.67 ppm. The presence of the solvent molecules in the structure of the materials can be observed as additional peaks (all labeled in Fig. 4B). Furthermore, the positions of FLU peaks in the solvate spectra are largely similar to the positions of FLU peaks in form I. The minor spectral differences observed between type I solvates and FLU form I are 1 ppm deshielding of carbon C3 and 1 ppm shielding of carbon C6 in FLU form I spectrum. These can be explained by FLU packing differences between both structures.

Thermal analysis. The thermal behavior of type I solvates was investigated using DSC and TGA (Fig. 4D). Desolvation of solvates was found to start at RT, right after removing the crystal from the solution, hence the measurements were started immediately after harvesting the crystals. DSC thermograms of type I solvates displayed a one-step desolvation endotherm followed by subsequent melting at *ca*. 139 °C for all solvates. Interestingly, the maximum solvent release is not strictly related to the order of boiling points (bp) of the pure solvents. The desolvation processes are finished above the boiling points of the solvents (for FLU EtAc and FLU Tol at *ca.* 130 °C, for FLU BuON at 105

°C, and for FLU ACN I at *ca.* 95 °C). Different behavior can be observed for FLU DMSO (bp. 189 °C) and FLU BuOH I (bp. 117 °C) where desolvation starts at lower temperatures – 75.4 and 87.2 °C respectively and finishes at *ca.* 85 and 105 °C respectively. The relatively high desolvation temperature of FLU EtAc and FLU Tol may be explained by their higher stability in comparison to the other type I solvates. To the best of our knowledge, the type I crystal structure is the only achievable form for FLU EtAc and FLU TOL solvates, while FLU ACN I and FLU BuOH I easily recrystallize to type II solvates during suspension experiments. The latter indicates that type II solvates are thermodynamically stable at RT in the presence of solvent vapor. Thermogravimetric analysis of the FLU EtAc solvate shows a weight loss of 6.56% which is in agreement with previous studies[28] and corresponds to 0.25 mole of solvent per mole of FLU (calculated weight loss 6.71%). Similar results were obtained for FLU Tol, FLU DMSO, FLU BuOH I, and FLU BuON solvates indicating the same molar ratio as for the FLU EtAc solvate (Fig. 4D). Lower experimental mass losses (as compared with calculated values) can be related to the instability of the solvates under N_2 purge (i.e., solvent loss prior starting the measurement). For FLU ACN I solvate we obtained a 6.0% mass loss which corresponds to 0.5 mole of the solvent per 1 mole of FLU (calc. 6.27%). As ACN has the smallest molecular volume (43 $Å^3$) across the type I solvates (DMSO 67 $Å^3$; BuON 75 $Å^3$; BuOH 79 $Å^3$; EtAc 84 $Å^3$; Tol 94 $Å^3$ as calculated using Olex2 software[63]), it is not surprising that two ACN molecules can occupy the available space to stabilize the channel-like structure. This corroborates the previous findings that molecular volume of the solvent correlates to the molar ratio of the solvate.[19,20]

Fluconazole type II solvates

Suspension of FLU form I in DCM, ACN, nPrOH, and BuOH results in the formation of a second type of fluconazole solvates (Scheme 1). These solvates are formed easily at RT except for ACN solvate which requires additional heating to overcome the phase transition energy barrier. In contrary

to FLU ACN I and FLU BuOH I solvates, they are thermodynamically stable and preserve their structure when suspended in the solvent. Also, the FLU host conformation and framework structure is maintained after desolvation of the type II solvates (see below).

X-ray and crystal structure analysis. Crystals of type II solvate prepared via suspension create snowball-like agglomerates, hence we were not able to obtain crystals suitable for SCXRD. Materials were analyzed using PXRD and for DCM, ACN II, and nPrOH solvates crystal structures were determined from PXRD data. Simulated diffractograms of type II solvates agree with experimental traces (Fig. 6A). Type II solvates were found to crystallize in a $P\bar{4}2_1c$ space group with Z'=1 (FLU). Visualized void space (Fig. 7A) indicates that solvent molecules are located inside the channels parallel to the *c* axis. The FLU molecules create O−H···N hydrogen-bonded $R_2^2(14)$ dimers with a conformation largely similar to the conformation found in FLU form II (Fig. 7B-C). To evaluate the stability of the FLU framework structure samples of the solvates were kept in a vacuum oven (50 °C, vacuum -0.6 bar) for a maximum of 18 days and were monitored by PXRD and TGA (ESI Fig. S14). The obtained PXRD patterns were compared to the calculated PXRD patterns simulated for structures with and without solvent molecules. The experimental patterns recorded after 4, 8, and 18 days were found to be similar to the simulated patterns of type II structures without solvents with only slight differences in intensity. Yet, the TGA traces after 18 days showed a maximum of 0.35% (0.01 mole of solvent per 1 mol of FLU) of the solvent present (for the BuOH solvate, ESI Fig. S14). The structure is maintained along a wide range of solvent content which indicates weak bonding of the solvent to FLU molecules, identifying type II solvates as non-stoichiometric. Therefore, the host FLU structure may be considered as stable and a so-called "isomorphic desolvates" are formed as an effect of the desolvation process. However, in the case of DCM and ACN II solvates an additional reflection was observed at 2θ = 7.9 ° in the PXRD pattern which shows a partial phase transformation to form II. Further increase of temperature up to 90 °C led to complete desolvation as shown by the TGA traces (Fig. 6D). From PXRD analysis it was found that increased temperature or loss of the "last"

solvent molecule induces phase transformation of the solvate structure into FLU form II. Schematic representation of feasible structural changes required for the transition of FLU type II solvates to FLU form II are presented in Fig. 7D. After desolvation half of the FLU dimers have to be rotated by *ca.* 90 ° and torsional angels in all molecules require a slight change to form the Z'=2 asymmetric unit. FLU form II molecules form non-centrosymmetric dimers similarly to the dimers present in FLU type II solvates (ESI Fig. S15), hence it may be hypothesized that rotation of molecules takes place without hydrogen bond breaking. Similarities in local environment of FLU form II, type II solvates and the isomorphic desolvate are corroborated with both FTIR and solid-state NMR spectra.

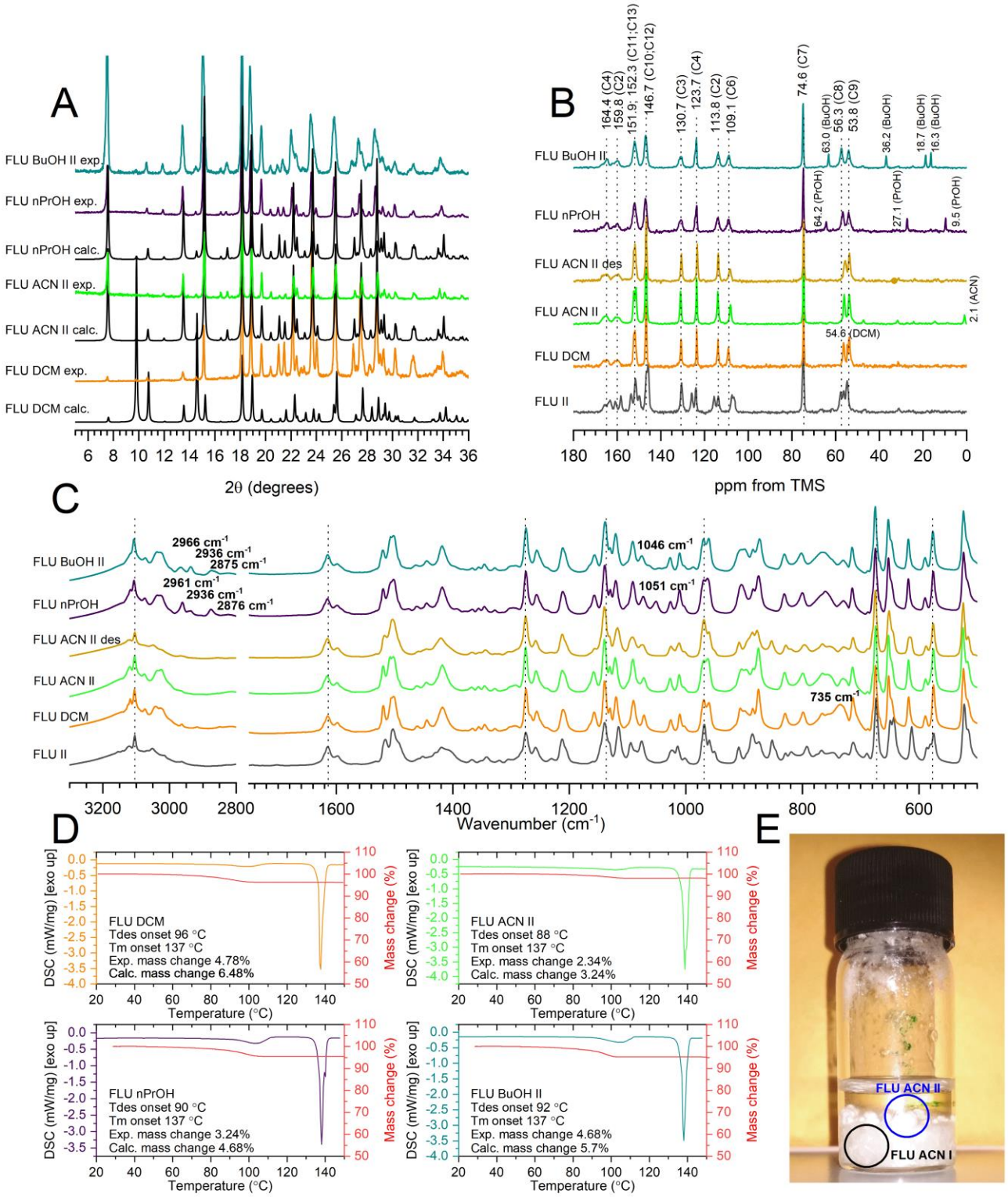

Figure 6. Experimental and calculated PXRD patterns of type II FLU solvates. B. ^{13}C CP/MAS NMR spectra of type II FLU solvates. C. FTIR spectra of type II FLU solvates with peaks assigned to the solvents marked with stars. D. DSC and TGA thermograms of type II FLU solvates. E. Snowball

morphology of ACN type II solvate (blue) growing in a suspension of ACN type I solvate (black) (see ESI Figure S13 for microscopic images showing morphology of both forms).

FTIR and solid-state NMR analysis. Recorded FTIR spectra of type II solvates display similar peak positions and intensities resulting from the isostructurality of the examined materials (Fig. 6C, full peak assignment ESI Table S5). Although the structural relationship between FLU type II solvates and FLU form II can be identified based on the FTIR spectral similarities (see ESI Table S5) several unique peaks that can be assigned to solvent molecules were identified in the FTIR spectra of type II solvates (ESI Table S5).

The ^{1}H-^{13}C solid-state NMR spectra of type II FLU solvates display comparable peak positions due to the isostructurality of the obtained materials. The experimental and calculated chemical shifts for FLU DCM solvate agreed with a RMSD value of 1.73 ppm. The presence of the solvent molecules in the structure of the materials can be observed as additional peaks marked in the spectra (Figure 6B). Type II solvate (Z'=1) spectra and the spectrum of the structurally related FLU form II (Z'=2) show differences in the number of peaks which is evident as two conformations of FLU molecules can be found in FLU form II. However, the positions of FLU peaks in the solvate spectra are largely similar to those assigned to one of the FLU molecules (pink molecule in Fig. 3B and 7C) in form II. This can be explained by the matching conformations of FLU molecules in both structures as well as by the presence of O−H···N hydrogen-bonded $R_2^2(14)$ dimers. The most noticeable spectral difference observed between both molecules of type II solvates and FLU form II is the 1.7 ppm deshielding of carbon C6 in FLU type II solvate spectra which may be explained by the slight change in proximity between carbon C6 and the electronegative N3 site of an adjacent molecule (3.219-3.226 Å in type II solvates; 3.298 Å in FLU form II).

Thermal analysis. DSC thermograms of type II solvates display a one-step desolvation followed by subsequent melting with onset at *ca.* 137 °C for all solvates (Fig. 6D). Despite significantly different boiling points of the used solvents, a similar desolvation temperature was recorded for each

type II solvate, indicating a similar strength of the host-guest interactions and identical host-host interactions. From the TGA traces it was found that the stoichiometry of type II solvates equals 0.25 mol of solvent per 1 mole of FLU (Fig. 6D). The solvent content of ACN solvate II is half of that in ACN solvate I. This was also corroborated with solid-state NMR results, where the integral ratio between carbons C7 and ACN in type I and II solvates was approximately 2:1 and 4:1, respectively.

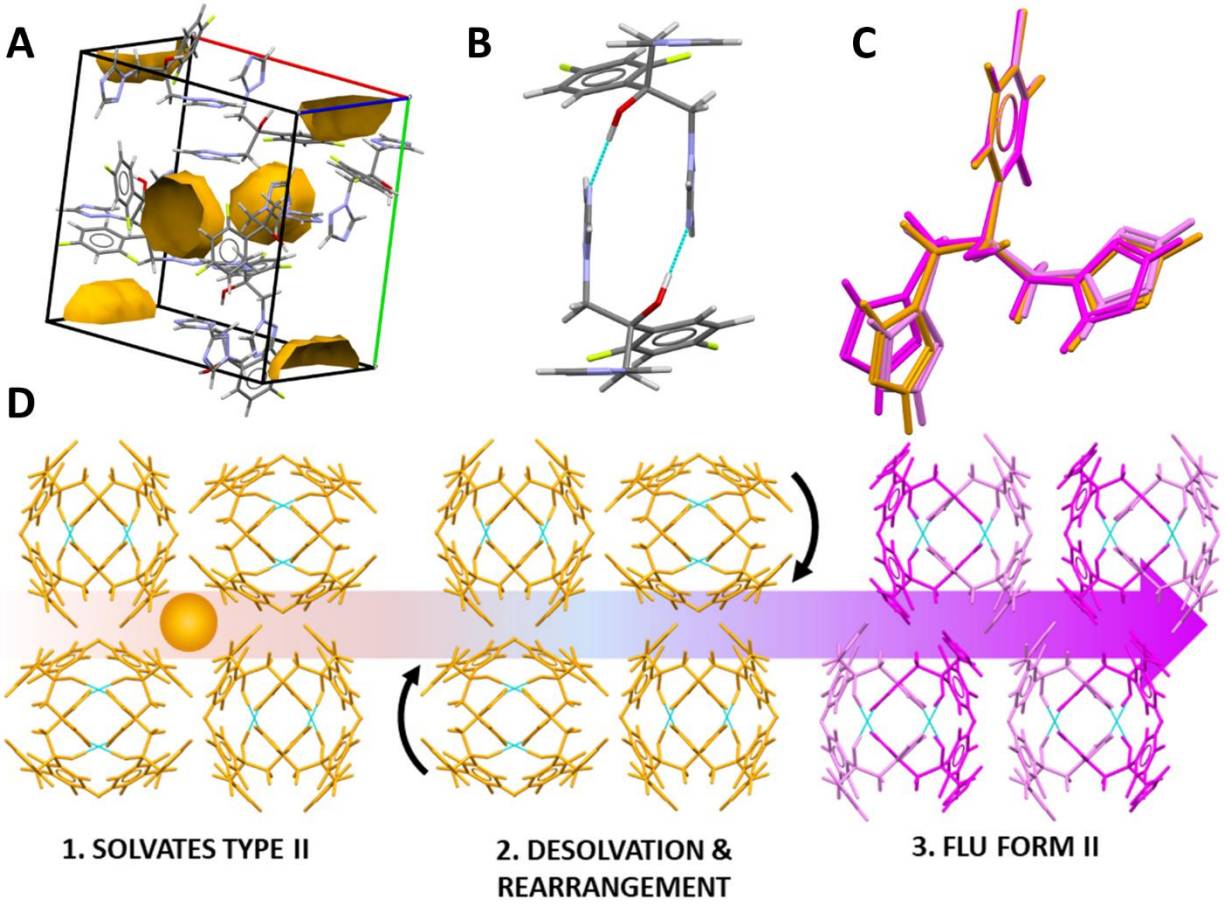

Figure 7. A. Packing of type II FLU solvates (as represented by FLU DCM). B. Hydrogen bonded dimers of type II FLU solvates. C. Overlay of FLU molecules in form II (pink and magenta) and type II solvates (orange). D. Proposed schematic representation of chain rearrangement during desolvation of FLU type II solvates.

Fluconazole solvates with ACT and TCM

Macroscopic investigations of crystals obtained from suspending FLU form I in ACT and TCM showed snowball-like morphology which is similar to the type II solvates. Formation of solvates was confirmed by the presence of peaks assigned to the solvents in FTIR and ^{1}H-^{13}C CP/MAS NMR spectra (ESI Figure S16). The PXRD measurements were performed using either a wet paste combined with a quick scan (0.1 s per step) or dried crystals with a regular setup due to the quick loss of solvent noticed. The transition from a wet paste to the dried crystals powder resulted in significant changes in PXRD patterns. The wet ACT solvate exhibits a distinct peak at $2\Theta = 5.9$ °. Drying of the material resulted in the appearance of a new peak at $2\Theta = 7.8$ ° which is absent in the wet TCM material. Reflections from the obtained materials could be assigned to neither FLU type II solvates nor FLU neat polymorphs patterns. The instability of the solid state forms did not allow us to derive the stoichiometric ratio of the potential solvate based on the TGA measurements. NMR and FTIR measurements sensitive to the local molecular environment show similarities in comparison to FLU type II solvates. The ^{1}H-^{13}C CP/MAS solid-state NMR spectra of ACT and TCM solvates displayed similar peak arrangements to FLU type II solvates. The obtained NMR spectra of ACT and TCM solvates displayed slight shifts of the aromatic ring peaks at 107.5 (C2), 113.2 (C6) and 124.8 ppm (C4) as compared to the solid-state NMR spectrum of the DCM solvate (ESI Fig. S16). The obtained FTIR spectra of the gently dried materials also confirm solvate formation (ESI Fig. S16). For dry ACT and TCM samples no solvent peaks were observed in both FTIR and solid-state NMR spectra, while the resulting FTIR spectra are similar to the spectra of the dry DCM materials.

Conclusions

Cooling and suspension crystallisation using 14 organic solvents were applied in order to perform a thorough investigation of solvent mediated phase transformations of fluconazole. Low molecular weight alcohols (MeOH, EtOH, isPrOH) and DMF favour the formation of neat FLU polymorphs. The obtained form – I, II, III or IV – depends on the crystallization conditions i.e.

supersaturation, temperature, or agitation. Form I and II can be produced through cooling crystallisation with careful control of the crystallisation temperature and drug supersaturation with respect to form I at RT. Form I crystallizes from isPrOH at $\sigma \approx 0.24$ and from MeOH ($\sigma \approx -0.59$ at RT and $\sigma \approx -0.08$ at ice bath temperature, EtOH ($\sigma \approx 0.29$) and DMF ($\sigma \approx 0.59$) with possible concomitant crystallisation of form II. At higher supersaturation (MeOH, $\sigma \approx 0.32$; EtOH $\sigma \approx 0.91$; isPrOH $\sigma \approx 1.44$ or DMF $\sigma \approx 0.81$) form II crystallizes preferentially. Suspension crystallisation results in formation of FLU form III or IV depending on additional stirring or lack thereof. The crystallisation conditions require particular attention considering the conformational similarity of fluconazole molecules across FLU I, II, and III and the possibility of concomitant crystallisation that may be due to similar solubility of these forms in alcohols and NNDMF. Revisiting the formation of form IV through slurrrying in BuON using form I as the initial form, we found form III as an intermediate phase that agrees with its slightly higher solubility as compared to form IV. Additionally the phase transtion to form IV can be attained through DMSO, MeOH, EtOH, and DMF suspension.

Two types of isostructural channel solvates of FLU were obtained for the first time, depending on crystallization conditions. Type I solvates were prepared by cooling crystallization in Tol, ACN, DMSO, BuOH and BuON and were found to be isostructural with a previously reported EtAc solvate. Formation of type II solvates was observed in DCM, ACN, nPrOH, and BuOH during suspension crystallization. NMR and FTIR analysis indicate that type II solvates can be obtained additionally using TCM and ACT. The solubility studies at RT showed the higher saturation solubility of type I solvates as compared with type II solvates explaining the stability relationship between FLU solvate types. For both types of solvates desolvation pathways were proposed. Desolvation of type I solvates leads to formation of FLU form I by rearrangement of hydrogen bonded chains. In type II solvates desolvation leads to formation of an isomorphic desolvate at first, with subsequent rearrangement of hydrogen bonded dimers and a phase transition into form II. Pairing solvent mediated phase transformation with structural analysis complemented with solid-state NMR supported by DFT-D

calculations allowed us to elucidate for the first time the interrelations and transformation pathways of FLU solid forms. This works proves that with increasing structural complexity, molecular weight and higher logP of new drug candidates careful control over crystallization conditions is essential to fully understand the solid-state landscape of highly flexible pharmaceuticals.

ASSOCIATED CONTENT

The Supporting Information is available at:

Literature and current work nomenclature and comparison (Table S1, Figure S1); solvents used in the study (Table S2); FLU forms solubility data in different solvents and their mixtures with water (Tables S3-S4); recrystallisation of FLU form II from melted sample – PXRD patterns, NMR spectra, DSC thermogram (Figures S2-S4); PXRD, FTIR, DSC and TGA analysis of FLU forms I, II, III and IV (Figures S5-S12); FTIR and NMR of FLU polymorphs and solvates analysis (Table S5); experimental and CASTEP calculated ^{13}C chemical shifts of FLU polymorphs and solvates (Table S6); crystal morphology of solvates type I and type II (Figure S13); stability of FLU type II solvates– PXRD patterns and TGA thermograms (Figure S14) and comparison of FLU hydrogen bonded dimers of form II and DCM solvate (Figure S15); ACT and TCM solvates – PXRD patterns, ^{13}C solid state NMR and FTIR spectra (Figure S16); fluconazole type II solvates– structure solution with final observed, calculated and difference profiles for the Rietveld refinement of FLU DCM solvate, FLU ACN solvate and FLU nPrOH solvate (Figure S17).

AUTHOR INFORMATION

Corresponding Author

*Karol P. Nartowski; Address: Borowska 211A, 50-556 Wroclaw, Poland; Phone: (+48) 71 784 05 69; E-mail: karol.nartowski@umed.wroc.pl

Author Contributions

The manuscript was written through contributions of all authors. All authors have given approval to the final version of the manuscript.

Funding Sources

This project was funded by National Science Centre in Poland via research grant UMO-2020/01/Y/ST4/00101 (AJD PhD scholarship).
This research was funded with national funds for scientific research by the Ministry of Science and Higher Education, Poland (SUB.D190.21.098).

ACKNOWLEDGEMENT

K.P.N., M.N. and A.J.D. thank the Laboratory of Elemental Analysis and Structural Research at the Faculty of Pharmacy at Wroclaw Medical University for the access to PXRD, DSC, TG and FTIR instruments. A.J.D. thanks National Science Centre in Poland for postgraduate scholarship via MOZART grant (UMO-2020/01/Y/ST4/00101). K.P.N. is grateful to National Science Centre in Poland and Ministry of Science and Higher Education for financial support enabling his research visits to UEA solid-state NMR facility. Marta Kozakiewicz-Latała is acknowledge for her assistance with HPLC analysis.

References

(1) Censi, R.; Di Martino, P. Polymorph Impact on the Bioavailability and Stability of Poorly Soluble Drugs. *Molecules* **2015**, *20* (10), 18759–18776. https://doi.org/10.3390/molecules201018759.

(2) Griesser, U. J. The Importance of Solvates. In *Polymorphism in the Pharmaceutical Industry*; Wiley-VCH Verlag GmbH & Co. KGaA: Weinheim, FRG, 2006; pp 211–233. https://doi.org/10.1002/3527607889.ch8.

(3) INTERNATIONAL COUNCIL FOR HARMONISATION OF TECHNICAL REQUIREMENTS FOR PHARMACEUTICALS FOR HUMAN. ICH guideline Q3C (R6) on impurities: guideline for residual solvents https://database.ich.org/sites/default/files/Q3C-R6_Guideline_ErrorCorrection_2019_0410_0.pdf (accessed May 7, 2021).

(4) Bhardwaj, R. M.; McMahon, J. A.; Nyman, J.; Price, L. S.; Konar, S.; Oswald, I. D. H.; Pulham, C. R.; Price, S. L.; Reutzel-Edens, S. M. A Prolific Solvate Former, Galunisertib, under the Pressure of Crystal Structure Prediction, Produces Ten Diverse Polymorphs. *J. Am. Chem. Soc.* **2019**, *141* (35), 13887–13897. https://doi.org/10.1021/jacs.9b06634.

(5) Mirmehrabi, M.; Rohani, S. An Approach to Solvent Screening for Crystallization of Polymorphic Pharmaceuticals and Fine Chemicals. *J. Pharm. Sci.* **2005**, *94* (7), 1560–1576. https://doi.org/10.1002/jps.20371.

(6) Shi, P.; Xu, S.; Du, S.; Rohani, S.; Liu, S.; Tang, W.; Jia, L.; Wang, J.; Gong, J. Insight into Solvent-Dependent Conformational Polymorph Selectivity: The Case of Undecanedioic Acid. *Cryst. Growth Des.* **2018**, *18* (10), 5947–5956. https://doi.org/10.1021/acs.cgd.8b00738.

(7) Du, W.; Yin, Q.; Gong, J.; Bao, Y.; Zhang, X.; Sun, X.; Ding, S.; Xie, C.; Zhang, M.; Hao, H. Effects of Solvent on Polymorph Formation and Nucleation of Prasugrel Hydrochloride. *Cryst. Growth Des.* **2014**, *14* (9), 4519–4525. https://doi.org/10.1021/cg5006067.

(8) Zhang, T.; Liu, Y.; Du, S.; Wu, S.; Han, D.; Liu, S.; Gong, J. Polymorph Control by Investigating the Effects of Solvent and Supersaturation on Clopidogrel Hydrogen Sulfate in Reactive Crystallization. *Cryst. Growth Des.* **2017**, *17* (11), 6123–6131.

https://doi.org/10.1021/acs.cgd.7b01311.

(9) Nartowski, K. P.; Karabin, J.; Morritt, A. L.; Nowak, M.; Fábián, L.; Karolewicz, B.; Khimyak, Y. Z. Solvent Driven Phase Transitions of Acyclovir – the Role of Water and Solvent Polarity. *CrystEngComm* **2019**, *21* (13), 2180–2192. https://doi.org/10.1039/C8CE01814F.

(10) Mattei, A.; Li, T. Nucleation of Conformational Polymorphs: A Computational Study of Tolfenamic Acid by Explicit Solvation. *Cryst. Growth Des.* **2014**, *14* (6), 2709–2713. https://doi.org/10.1021/cg5000815.

(11) Yu, L. Polymorphism in Molecular Solids: An Extraordinary System of Red, Orange, and Yellow Crystals. *Acc. Chem. Res.* **2010**, *43* (9), 1257–1266. https://doi.org/10.1021/ar100040r.

(12) Lévesque, A.; Maris, T.; Wuest, J. D. ROY Reclaims Its Crown: New Ways To Increase Polymorphic Diversity. *J. Am. Chem. Soc.* **2020**, *142* (27), 11873–11883. https://doi.org/10.1021/jacs.0c04434.

(13) Lemmerer, A.; Adsmond, D. A.; Esterhuysen, C.; Bernstein, J. Polymorphic Co-Crystals from Polymorphic Co-Crystal Formers: Competition between Carboxylic Acid···Pyridine and Phenol···Pyridine Hydrogen Bonds. *Cryst. Growth Des.* **2013**, *13* (9), 3935–3952. https://doi.org/10.1021/cg4006357.

(14) Jia, L.; Yin, Q.; Zhou, L.; Zhang, X.; Wang, C.; Du, W.; Zhou, L. Insights into the Mechanism of Concomitant Nucleation of Form II and Ethanol Solvate of Spironolactone in Cooling Crystallization. *RSC Adv.* **2018**, *8* (18), 9697–9706. https://doi.org/10.1039/C7RA13094E.

(15) Cruz-Cabeza, A. J.; Bernstein, J. Conformational Polymorphism. *Chem. Rev.* **2014**, *114* (4), 2170–2191. https://doi.org/10.1021/cr400249d.

(16) Zhang, C.; Kersten, K. M.; Kampf, J. W.; Matzger, A. J. Solid-State Insight Into the Action of

a Pharmaceutical Solvate: Structural, Thermal, and Dissolution Analysis of Indinavir Sulfate Ethanolate. *J. Pharm. Sci.* **2018**, *107* (10), 2731–2734. https://doi.org/10.1016/j.xphs.2018.06.020.

(17) Price, C. P.; Glick, G. D.; Matzger, A. J. Dissecting the Behavior of a Promiscuous Solvate Former. *Angew. Chemie - Int. Ed.* **2006**, *45* (13), 2062–2066. https://doi.org/10.1002/anie.200503533.

(18) Werner, J. E.; Swift, J. A. Organic Solvates in the Cambridge Structural Database. *CrystEngComm* **2021**, *2000* (October 1998). https://doi.org/10.1039/D0CE01749C.

(19) Braun, D. E.; Gelbrich, T.; Griesser, U. J. Experimental and Computational Approaches to Produce and Characterise Isostructural Solvates. *CrystEngComm* **2019**, *21* (36), 5533–5545. https://doi.org/10.1039/C9CE00856J.

(20) Yang, H.; Yang, Y.; Jia, L.; Tang, W.; Xu, S.; Du, S.; Li, M.; Gong, J. The Phase Transformation and Formation Mechanism of Isostructural Solvates: A Case Study of Azoxystrobin. *Cryst. Growth Des.* **2019**, *19* (3), 1550–1558. https://doi.org/10.1021/acs.cgd.8b01144.

(21) Beloborodova, A. A.; Minkov, V. S.; Rychkov, D. A.; Rybalova, T. V.; Boldyreva, E. V. First Evidence of Polymorphism in Furosemide Solvates. *Cryst. Growth Des.* **2017**, *17* (5), 2333–2341. https://doi.org/10.1021/acs.cgd.6b01191.

(22) Takieddin, K.; Khimyak, Y. Z.; Fábián, L. Prediction of Hydrate and Solvate Formation Using Statistical Models. *Cryst. Growth Des.* **2016**, *16* (1), 70–81. https://doi.org/10.1021/acs.cgd.5b00966.

(23) Leeson, P. D.; Springthorpe, B. The Influence of Drug-like Concepts on Decision-Making in

Medicinal Chemistry. *Nat. Rev. Drug Discov.* **2007**, *6* (11), 881–890. https://doi.org/10.1038/nrd2445.

(24) World Health Organization. WHO Model Lists of Essential Medicines https://list.essentialmeds.org/ (accessed May 7, 2021).

(25) Pappas, P. G.; Kauffman, C. A.; Andes, D. R.; Clancy, C. J.; Marr, K. A.; Ostrosky-Zeichner, L.; Reboli, A. C.; Schuster, M. G.; Vazquez, J. A.; Walsh, T. J.; Zaoutis, T. E.; Sobel, J. D. Executive Summary: Clinical Practice Guideline for the Management of Candidiasis: 2016 Update by the Infectious Diseases Society of America. *Clin. Infect. Dis.* **2016**, *62* (4), 409–417. https://doi.org/10.1093/cid/civ1194.

(26) Grudzień, M.; Król, A.; Paterek, G.; Stępień, K.; Pluciński, F.; Mazurek, A. P. The Structure–Bioavailability Approach in Antifungal Agents. *Eur. J. Med. Chem.* **2009**, *44* (5), 1978–1981. https://doi.org/10.1016/j.ejmech.2008.10.028.

(27) Richardson, K. U.S. Patent US4404216A, 1983.

(28) Caira, M. R.; Alkhamis, K. A.; Obaidat, R. M. Preparation and Crystal Characterization of a Polymorph, a Monohydrate, and an Ethyl Acetate Solvate of the Antifungal Fluconazole. *J. Pharm. Sci.* **2004**, *93* (3), 601–611. https://doi.org/10.1002/jps.10541.

(29) Karanam, M.; Dev, S.; Choudhury, A. R. New Polymorphs of Fluconazole: Results from Cocrystallization Experiments. *Cryst. Growth Des.* **2012**, *12* (1), 240–252. https://doi.org/10.1021/cg201005y.

(30) Basford, P. A.; Back, K. R.; Cram, M.; Docherty, R.; Davey, R. J.; Cruz-Cabeza, A. J. Impact of Crystal Structure and Molecular Conformation on the Hydration Kinetics of Fluconazole. *Cryst. Growth Des.* **2019**, *19* (12), 7193–7205. https://doi.org/10.1021/acs.cgd.9b01066.

(31) Basford, P. A.; Cameron, C. A.; Cruz-Cabeza, A. J. Conformational Change Initiates Dehydration in Fluconazole Monohydrate. *Cryst. Growth Des.* **2020**, *20* (9), 6044–6056. https://doi.org/10.1021/acs.cgd.0c00768.

(32) Alkhamis, K. A.; Obaidat, A. A.; Nuseirat, A. F. Solid-State Characterization of Fluconazole. *Pharm. Dev. Technol.* **2002**, *7* (4), 491–503. https://doi.org/10.1081/PDT-120015052.

(33) Desai, S. R.; Shaikh, M. M.; Dharwadkar, S. R. Thermoanalytical Study of Polymorphic Transformation in Fluconazole Drug. *Thermochim. Acta* **2002**, *399* (1–2), 81–89. https://doi.org/10.1016/S0040-6031(02)00451-3.

(34) Kreidl, J.; Czibula, L.; Szantay, C.; Farkas, J.; Juhasz, I. D.; Hegedus, I.; Papp, E. W.; Badgy, J. N.; Piller, A. Patent WO2002076955A1, 2002.

(35) Kastelic, J.; Hodnik, Z.; Šket, P.; Plavec, J.; Lah, N.; Leban, I.; Pajk, M.; Planinšek, O.; Kikelj, D. Fluconazole Cocrystals with Dicarboxylic Acids. *Cryst. Growth Des.* **2010**, *10* (11), 4943–4953. https://doi.org/10.1021/cg1010117.

(36) Kastelic, J.; Lah, N.; Kikelj, D.; Leban, I. A 1:1 Cocrystal of Fluconazole with Salicylic Acid. *Acta Crystallogr. Sect. C Cryst. Struct. Commun.* **2011**, *67* (9), o370–o372. https://doi.org/10.1107/S0108270111031155.

(37) Dayo Owoyemi, B. C.; da Silva, C. C. P.; Souza, M. S.; Diniz, L. F.; Ellena, J.; Carneiro, R. L. Fluconazole: Synthesis and Structural Characterization of Four New Pharmaceutical Cocrystal Forms. *Cryst. Growth Des.* **2019**, acs.cgd.8b01194. https://doi.org/10.1021/acs.cgd.8b01194.

(38) Surov, A. O.; Voronin, A. P.; Vasilev, N. A.; Churakov, A. V.; Perlovich, G. L. Cocrystals of Fluconazole with Aromatic Carboxylic Acids: Competition between Anhydrous and Hydrated

Solid Forms. *Cryst. Growth Des.* **2020**, *20* (2), 1218–1228. https://doi.org/10.1021/acs.cgd.9b01490.

(39) Gu, C. H.; Li, H.; Gandhi, R. B.; Raghavan, K. Grouping Solvents by Statistical Analysis of Solvent Property Parameters: Implication to Polymorph Screening. *Int. J. Pharm.* **2004**, *283* (1–2), 117–125. https://doi.org/10.1016/j.ijpharm.2004.06.021.

(40) Clark, S. J.; Segall, M. D.; Pickard, C. J.; Hasnip, P. J.; Probert, M. I. J.; Refson, K.; Payne, M. C. First Principles Methods Using CASTEP. *Zeitschrift für Krist. - Cryst. Mater.* **2005**, *220* (5–6), 567–570. https://doi.org/10.1524/zkri.220.5.567.65075.

(41) Nicoud, L.; Licordari, F.; Myerson, A. S. Estimation of the Solubility of Metastable Polymorphs: A Critical Review. *Cryst. Growth Des.* **2018**, *18* (11), 7228–7237. https://doi.org/10.1021/acs.cgd.8b01200.

(42) Schall, J. M.; Capellades, G.; Myerson, A. S. Methods for Estimating Supersaturation in Antisolvent Crystallization Systems. *CrystEngComm* **2019**, *21* (38), 5811–5817. https://doi.org/10.1039/C9CE00843H.

(43) Markvardsen, A. J.; David, W. I. F.; Johnson, J. C.; Shankland, K. A Probabilistic Approach to Space-Group Determination from Powder Diffraction Data. *Acta Crystallogr. Sect. A Found. Crystallogr.* **2001**, *57* (1), 47–54. https://doi.org/10.1107/S0108767300012174.

(44) David, W. I. F.; Shankland, K.; van de Streek, J.; Pidcock, E.; Motherwell, W. D. S.; Cole, J. C. DASH : A Program for Crystal Structure Determination from Powder Diffraction Data. *J. Appl. Crystallogr.* **2006**, *39* (6), 910–915. https://doi.org/10.1107/S0021889806042117.

(45) Rietveld, H. M. A Profile Refinement Method for Nuclear and Magnetic Structures. *J. Appl. Crystallogr.* **1969**, *2* (2), 65–71. https://doi.org/10.1107/S0021889869006558.

(46) Coelho, A. Topas Academic Coelho Software. Brisbane 2016.

(47) CrysAlis CCD and CrysAlis Red 1.171.38.43. Rigaku Oxford Diffraction 2015.

(48) Sheldrick, G. M. SHELXT – Integrated Space-Group and Crystal-Structure Determination. *Acta Crystallogr. Sect. A Found. Adv.* **2015**, *71* (1), 3–8. https://doi.org/10.1107/S2053273314026370.

(49) Sheldrick, G. M. Crystal Structure Refinement with SHELXL. *Acta Crystallogr. Sect. C Struct. Chem.* **2015**, *71* (1), 3–8. https://doi.org/10.1107/S2053229614024218.

(50) Björkman, T. CIF2Cell: Generating Geometries for Electronic Structure Programs. *Comput. Phys. Commun.* **2011**, *182* (5), 1183–1186. https://doi.org/10.1016/j.cpc.2011.01.013.

(51) Perdew, J. P.; Burke, K.; Ernzerhof, M. Generalized Gradient Approximation Made Simple. *Phys. Rev. Lett.* **1996**, *77* (18), 3865–3868. https://doi.org/10.1103/PhysRevLett.77.3865.

(52) Vanderbilt, D. Soft Self-Consistent Pseudopotentials in a Generalized Eigenvalue Formalism. *Phys. Rev. B* **1990**, *41* (11), 7892–7895. https://doi.org/10.1103/PhysRevB.41.7892.

(53) Tkatchenko, A.; Scheffler, M. Accurate Molecular Van Der Waals Interactions from Ground-State Electron Density and Free-Atom Reference Data. *Phys. Rev. Lett.* **2009**, *102* (7), 073005. https://doi.org/10.1103/PhysRevLett.102.073005.

(54) Pickard, C. J.; Mauri, F. All-Electron Magnetic Response with Pseudopotentials: NMR Chemical Shifts. *Phys. Rev. B* **2001**, *63* (24), 245101. https://doi.org/10.1103/PhysRevB.63.245101.

(55) Yates, J. R.; Pickard, C. J.; Mauri, F. Calculation of NMR Chemical Shifts for Extended Systems Using Ultrasoft Pseudopotentials. *Phys. Rev. B* **2007**, *76* (2), 24401. https://doi.org/10.1103/PhysRevB.76.024401.

(56) Kreidl, J.; Czibula, L.; Szantay, C.; Farkas, J.; Juhasz, I. D.; Hegedus, I.; Papp, E. W.; Badgy, J. N.; Piller, A. U.S. Patent, US 007094904 B2, 2006. https://doi.org/10.1145/634067.634234.

(57) Gu, X. J.; Jlang, W. Characterization of Polymorphic Forms of Fluconazole Using Fourier Transform Raman Spectroscopy. *J. Pharm. Sci.* **1995**, *84* (12), 1438–1441. https://doi.org/10.1002/jps.2600841210.

(58) Dash, A. K.; Elmquist, W. F. Fluconazole; 2001; Vol. 21, pp 67–113. https://doi.org/10.1016/S1075-6280(01)27005-0.

(59) Chandrasekaran, K.; Thilak Kumar, R. Structural, Spectral, Thermodynamical, NLO, HOMO, LUMO and NBO Analysis of Fluconazole. *Spectrochim. Acta - Part A Mol. Biomol. Spectrosc.* **2015**, *150*, 974–991. https://doi.org/10.1016/j.saa.2015.06.018.

(60) Gu, C.-H.; Young, V.; Grant, D. J. W. Polymorph Screening: Influence of Solvents on the Rate of Solvent-Mediated Polymorphic Transformation. *J. Pharm. Sci.* **2001**, *90* (11), 1878–1890. https://doi.org/10.1002/jps.1137.

(61) Lo, J. B.; Mackay, G. G.; Puz, M. J. UK Patent Application GB 2270521A. **1994**.

(62) Alkhamis, K. A.; Salem, M. S.; Obaidat, R. M. Comparison between Dehydration and Desolvation Kinetics of Fluconazole Monohydrate and Fluconazole Ethylacetate Solvate Using Three Different Methods. *J. Pharm. Sci.* **2006**, *95* (4), 859–870. https://doi.org/10.1002/jps.20605.

(63) Dolomanov, O. V.; Bourhis, L. J.; Gildea, R. J.; Howard, J. A. K.; Puschmann, H. OLEX2: A Complete Structure Solution, Refinement and Analysis Program. *urn:issn:0021-8898* **2009**, *42* (2), 339–341. https://doi.org/10.1107/S0021889808042726.